Soft Matter

PAPER

Domain expansion dynamics in stratifying foam films: experiments†

Yiran Zhang and Vivek Sharma*

The stability, rheology and applications of foams, emulsions and colloidal sols depend on the hydrodynamics and thermodynamics of thin liquid films that separate bubbles, drops and particles respectively. Thin liquid films containing micelles, colloidal particles, liquid crystals or polyelectrolyte–surfactant mixtures exhibit step-wise thinning or stratification, often attributed to the layer-by-layer removal of the aforementioned supramolecular structures. Stratification proceeds through emergence and growth of thinner circular domains within a thicker film, and the domain expansion dynamics are the focus of this study. Domain and associated thickness variation in foam films made from sodium dodecyl sulfate (SDS) micellar solutions are examined using a Scheludko-type cell with a novel technique we call Interferometry Digital Imaging Optical Microscopy (IDIOM). Below 100 nm, stratification and drainage cause a thickness-dependent variation in reflected light intensity, visualized as progressively darker shades of gray. We show that the domain expansion dynamics exhibit two distinct growth regimes with characteristic scaling laws. Initially, the radius of the isolated domains grows with square root time, and the expansion rate can be characterized by an apparent diffusion constant. In contrast, after a section of the expanding domain coalesces with the Plateau border, the contact line between domain and the surrounding thicker region moves a constant velocity. We show that a similar transition from a constant diffusivity to a constant velocity regime is also realized when a topological instability occurs at the contact line between the growing thinner isolated domain and the surrounding thicker film. Though several studies have focused on the expansion dynamics of isolated domains that exhibit a diffusion-like scaling, the change in expansion kinetics observed after domains contact with the Plateau border has not been reported and analyzed before.

1. Introduction

Liquid foams exhibit a range of complex and unique properties that make them nearly indispensible for numerous applications in our daily lives and in industrial processes.[1–5] Foams are colloidal dispersions of tightly packed gas bubbles in a continuous liquid (or solid) phase. Structurally, as foams consist of thin films separated by gas pockets, the stability, lifetime, rheology and applications of liquid foams are intimately linked to the drainage and rupture kinetics of thin liquid films.[6–10] Thus, foams are similar to emulsions and colloidal sols, as their stability and rheology also depend on the hydrodynamics and thermodynamics of thin liquid films that separate drops and particles respectively.[6–11] In an absolute sense, foams (and in fact all colloidal dispersions) are thermodynamically unstable,[11] though practically speaking, systems can be categorized as relatively short-lived or reasonably long-lived (timescale of minutes to hours to years). Slower drainage rates and more stable foams are desirable in firefighting,[12,13] mining industry,[14] certain foods and beverages,[15] and cosmetics[16,17] among others. In striking contrast, rapid drainage and disappearance of foams is preferred in champagnes[18,19] and in undesirable aquatic foams created by water pollution.[20,21] Understanding and unraveling the physico-chemical mechanisms operative within thin liquid films that govern the lifetime and stability of aqueous foams is a longstanding challenge, and the underlying motivation for this study.

Representative examples of foam can be prepared simply by shaking an aqueous soap solution, or by blowing bubbles into it, or by pouring a glass of frothy beer! If such a foam head is allowed to stand for a while, on closer inspection, a transition from polyhedral-shaped bubbles of dry foam (low liquid fraction) at the top to the spherical bubbles of wet foam near bulk fluid can be recognized.[5] In dry foam, nearly plane–parallel thin films are linked to each other through thicker channels and nodes called Plateau borders,[5,22] and the experimental studies described in this paper aim to mimic drainage in such foam films.

Department of Chemical Engineering, University of Illinois at Chicago, Chicago, IL 60607, USA. E-mail: viveks@uic.edu

The drainage of liquid within the dry foam structure is primarily driven by capillary forces,[6–8,22–28] and the foam lifetime is prolonged if the rate of drainage is reduced by viscous (interfacial or bulk) contributions.[5,7,22] As film thickness approaches the molecular length-scales, or when interfacial regions begin to overlap, the drainage can be further enhanced or reduced by an additional contribution from surface forces[18,29–31] that provide an excess pressure called disjoining pressure, which acts normal to the surface. The foam lifetime is also prolonged if inter-bubble gas diffusion is inhibited.[5,25] Several reviews,[6,32,33] textbooks[5,10,11,25] and a recent themed issue in Soft Matter published in 2014 (and papers therein[34–37]) present a survey of the current state-of-the-art understanding in foams and emulsions; the mechanisms underlying foam stability and drainage feature as challenging problems in each one of them.

At the molecular level, foam films are often stabilized by amphiphilic surface-active agents (or surfactants) that spontaneously adsorb to the liquid/air interfaces, and typically, reduce the surface energy or tension associated with surfaces.[25,27,32] The surfactants determine the magnitude of both capillary pressure and disjoining pressure[18] and alter the rheological response of the interfaces as well as the bulk fluid.[23–27,32] Surface and bulk properties of surfactant solutions are concentration-dependent, though above a threshold value known as critical micelle concentration (cmc),[11,38] added surfactants spontaneously self-assemble into supramolecular structures called micelles. For thin films containing micelles, drainage proceeds in a non-monotonic, step-wise fashion called stratification,[28,39–42] in contrast to the monotonic thinning behavior exhibited by foam films made with surfactant concentrations below cmc. For the latter, the thickness variation of disjoining pressure can be described within the framework of DLVO theory[7,18,29,38] (named after Derjaguin, Landau, Verwey, and Overbeek). The DLVO forces include destabilizing, attractive London-van der Waals dispersion forces and stabilizing, repulsive, double layer electrostatic interactions.[29,38] In contrast, the disjoining pressure of micellar fluids includes an additional contribution referred to as supramolecular oscillatory structural forces.[18,43] The latter forces can nearly counterbalance capillary pressure at substantially higher thicknesses ($\sim$80 nm) than DLVO forces (significant only below $\sim$40 nm).[18] Mechanistically, stratification proceeds through expansion of thinner, visually darker, circular domains that spontaneously form within a thicker film of micellar fluid, and the overall drainage rate is reduced in comparison with non-stratifying films.[43,44] While many studies have focused on the equilibrium state of each thickness step and its relation to supramolecular structural components of disjoining pressure,[43,45–47] there are many unanswered questions regarding the physicochemical hydro-dynamics underlying stratification.[42,44,48–50] These are explored herein in the context of domain expansion dynamics.

Stratification in thin films made with surfactant solutions was first reported by Johonnott[51] in 1906 and soon after was examined by Perrin.[52] The domain expansion dynamics were first characterized by Kralchevsky, Nikolov, Wasan and Ivanov,[44] who reported that the area of an isolated circular, thinner domain, A_d increases linearly over time, t. Similar expansion dynamics with diffusion-like kinetics (for $A_d \propto t$ leads to radius $R \propto t^{0.5}$) are observed in the studies focused on the kinetics of domain expansion in micellar,[44,53] particulate,[54] and polyelectrolyte–surfactant films.[48–50] An isolated domain encounters the same driving force and resistance in all directions. In contrast, the expansion of domain after contact with Plateau border takes place under non-centro-symmetric driving force. We observe that in this regime, the expansion dynamics are no longer diffusive.

To the best of our knowledge, all the published studies[43,44,48–50,53–55] have focused exclusively on the expansion of a single isolated domain, far away from the Plateau border. There is a sheer lack of any experimental data on if and how expansion dynamics change when the expanding domain comes in contact with the Plateau border. The present study aims to fill that gap by visualizing and analyzing stratification kinetics and domain expansion dynamics in thin films made with aqueous micellar solutions of an anionic surfactant called sodium dodecyl sulfate (SDS). A novel technique called Interferometry Digital Imaging Optical Microscopy (IDIOM) is introduced for simultaneous measurement of thickness variation accompanying drainage and characterization of domain expansion dynamics. The technique is described briefly in the next section. Experiments on domain expansion dynamics for isolated domains growing far from the Plateau border are presented thereafter, and in agreement with the previous studies, the domain growth appears to be diffusive for isolated domains. Finally, the dynamics observed after expanding domain coalesces with the Plateau border are characterized and we believe, these are described for the first time.

2. Materials and methods

2.1. Materials: aqueous SDS solutions

Horizontal foam films are formed with aqueous solutions of sodium dodecyl sulfate (SDS) both below and above the critical micelle concentration (literature values range between 7–10 mM at 25 °C).[56] SDS (anionic, molecular weight of 288 Daltons, Sigma-Aldrich Co., St. Louis, MO, L6026, >99.0%) is used without further purification, and all solutions are prepared with deionized water with resistivity of 18.2 MΩ. It is well known that the presence of impurities or the presence of trace amounts of 1-dodecanol affect micellization, surface tension and interfacial rheology.[57,58] The concentration-dependent surface tension of aqueous SDS solutions measured using a maximum bubble pressure tensiometer shows a smooth transition near a cmc value of $c = 8.2$ mM, indicating that the as-made solutions are relatively free of impurities.[57,58] No electrolytes are added to the solution, for it is well known that high ionic content leads to suppression of the stratification phenomena.[28,39]

2.2. Thin film apparatus and imaging system

Drainage and stratification experiments were carried out in a Scheludko-type cell[9] (see the schematic included as Fig. 1). The test solution is loaded into a cylindrical cell of internal diameter $d_c = 1.6$ mm. Liquid is then slowly withdrawn from the biconcave drop to create a circular thin film at the center with
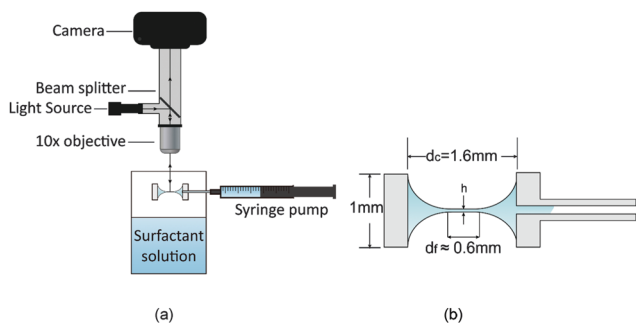
Fig. 1 Introducing Interferometry Digital Imaging Optical Microscopy (IDIOM) set-up for characterizing thin film hydrodynamics. (a) Schematic of the experimental setup. A combination of digital imaging and high-resolution optics allows both visualization and characterization of the stratification and drainage processes within a thin film. (b) Schematic of thin foam film formed within a cylindrical Scheludko-like cell by withdrawing liquid out from the sidearm. Both plane–parallel region and Plateau region are shown. After the required initial thickness is obtained, the film is allowed to drain freely. The images captured are analyzed to measure spatial and temporal variation in thickness (see text for details).

nearly plane–parallel interfaces (Fig. 1b). The withdrawal is stopped after the desired film diameter ($d_f \approx 0.6$ mm) is reached, and the fluid volume is then maintained constant throughout the drainage process. The film holding cell is placed within a closed container, in which air is saturated with the same test solution to minimize the effect of evaporation. In analogy with a horizontal film in dry foam, the thin film formed within the cell always stays in contact with a thicker meniscus region (referred to as Plateau border). Assuming perfect wetting of the inner wall of the cell holder and a small contact angle between the film and the border region, the capillary pressure can be estimated by:[39]

$$P_c \approx \frac{4\gamma d_c}{d_c{}^2 - d_f{}^2} \qquad (1)$$

Here γ is the surface tension of the solution ($\gamma \approx 36$ mN m^{-1} for SDS solutions above cmc, measured using a maximum bubble pressure tensiometer designed within the laboratory), d_c and d_f are the inner diameter of the cell and the diameter of the thin film, respectively, as shown in Fig. 1b. The typical capillary pressure in experiments described in this study is $P_c \approx 100$ Pa. In a series of papers, Wasan, Nikolov and coworkers[31,54,55] have argued that the stratification kinetics is itself influenced by the film size and curvature. To make a meaningful comparison between solutions with different surfactant and micellar concentration, we conducted experiments on films that are nearly plane–parallel and of similar size.

The reflected light intensity, I from a homogeneous film (after neglecting absorption, including multiple reflection and assuming zeroth order of interference) can be related to its thickness, h by using the following formula:[9]

$$h = \left(\frac{\lambda}{2n\pi}\right) \arcsin\left(\sqrt{\frac{\Delta}{1 + 4R(1 - \Delta)/(1 - R)^2}}\right) \qquad (2)$$

Here $\Delta = (I - I_{min})/(I_{max} - I_{max})$ is computed using the reflected light intensity, I measured at a particular spot, and I_{max} and I_{min} are the maximum and the minimum intensities measured for a given wavelength of light, λ. In eqn (2), the Fresnel coefficient $R = (n - 1)^2/(n + 1)^2$ is computed using the value of refractive index, n of the bulk solution (here $n = 1.33$). Prior studies[9,59,60] show that corrections based on the measured refractive index for different SDS concentrations, or based on calculations that treat foam as a multilayered structure are negligible and can be ignored. Interference occurs between the light rays reflected from the two liquid–air interfaces present in thin foam films. The phase difference between the interfering rays arises due to: (a) the path difference between the two rays which is determined by film thickness, angle of incidence and number of reflections within the film, and (b) a phase shift of π that always occurs on the reflection at air–liquid surface (where incident and reflected light lie in medium with lower refractive index). Even for black films that are only a few molecular-layers thick, light intensity modulated by interference provides a measure of film thickness.

The thin film is illuminated by white light, and the reflected light is recorded by high resolution DSLR camera (Nikon D5200). The camera is equipped with a precision microscope lens system (Navitar Zoom 6000, with added microscope objective). High-resolution videos and images of the stratification process are captured by this imaging system. The images are post-processed in MATLAB R2012a with specially written codes and using eqn (2), changes in the film thickness are computed from the intensity of reflected light. Conventionally a photodiode is used for measuring the reflected light intensity. In this study we use a novel approach that we have developed and termed as Interferometry Digital Imaging Optical Microscopy (IDIOM); this relies on the high quality sensors of the digital camera for measuring I (the reflected light intensity).

The principle underlying thickness determination by IDIOM can be described in brief as follows. Every pixel in the color image can be read as a composite of three intensities of red (wavelength $\lambda = 650$ nm), green ($\lambda = 546$ nm) and blue ($\lambda = 450$ nm) light, and each color channel has values in the range of 0–255. The intensities corresponding to the three channels correspond to the thickness-dependent reflected light intensity for each color, and these can be converted into the thickness of the foam film using eqn (2). While similar digital filtration and thickness determination using reflected light intensity has been used for measuring film thicknesses with thicker, colored soap films,[61,62] this is, we believe, the first application to thicknesses below 100 nm. The thickness h obtained is called the "equivalent film thickness",[63,64] which assumes refractive index in the thin film is homogenous and equal to the value of the bulk solution. A more detailed description of IDIOM, its resolution limits and detection efficiency, as well as improving the accuracy of thickness measurement will be presented in a separate article. In the present context, the technique allows us to map the thickness of the film with high spatial resolution (up to ~0.5 μm per pixel), which is advantageous in investigating the kinetics of the growth of circular domains of different thickness as described and discussed herein.

3. Results and discussion

3.1. Step-wise thinning of films formed with 100 mM aqueous SDS solution

Stratification within thin foam films formed from an aqueous micellar SDS solution (c = 100 mM; c/cmc $\approx$ 12) proceeds as shown in snapshots in Fig. 2a (see Movie S1 included as ESI†). Interference between light reflected from the two air–liquid
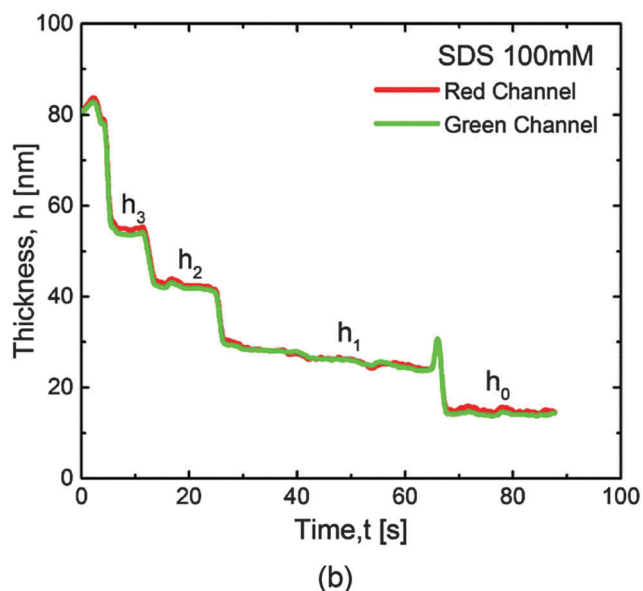

interfaces of the foam film with thickness, $h > 100$ nm creates colorful rings. The vibrant interference colors disappear below $h \approx 100$ nm. However, as the intensity of reflected light is dependent on thickness for $h < 100$ nm and various shades of gray can be perceived (see Fig. 2a), right up to the nearly black color characteristic of the thinnest films. Remarkably, in these micellar fluids, the thinning films display distinct regions with different shades of gray implying that regions of different thickness co-exist in the film (see Fig. 2a). Thinner (hence darker) circular domains spontaneously form and grow within the thicker film (see Movie S1, ESI†). The domain boundaries are sharp, and expansion of the domain continues till the thickness of entire film is reduced to the next thickness, smaller by a discrete value equal to the step size. The final black film formed after multiple thinning events can be stable for hours without rupturing.

The progressive thinning of foam film leads to intensity variations that provide quantitative determination of changes in thickness. The plot of thickness *versus* time reveals that thinning takes place in step-wise fashion (see Fig. 2b). For 100 mM SDS solution, the measurement shows a final thickness $h_0 = 14.6 \pm 0.6$ nm, and the height of each step is found to be constant with $\Delta h = 10.5 \pm 0.5$ nm. Intensities corresponding to red and green channels are analyzed separately, and a good agreement is found between the estimates made with the two different wavelengths, as shown in Fig. 2. The data from the blue channel is quite noisy and is not shown. The experiments were repeated at least five times for each of the six different SDS concentrations. Step-size and final black film thickness decrease with an increase in concentration and the number of steps increases with concentration. The concentration-dependence of the step-size (Δh), the final thickness of black film (h_0), as well as their measured values, are similar to those reported in the literature.[65,66]

3.2. Domain expansion kinetics: influence of the Plateau border

Stratification proceeds through formation and expansion of thinner, darker domains (see Movie S1, ESI†). At first, one or more domains grow without interacting with any neighboring domains or with the Plateau border. In many instances, a single darker domain emerges and grows till the thickness of the whole plane–parallel film is reduced to the next step in thickness. Domain area expansion dynamics was analyzed for five different concentrations, and a representative example of domain growth kinetics is shown in Fig. 3 for a 100 mM aqueous SDS solution.

We find that the expansion process invariably involves at least two distinct regimes: Regime A, expansion as an isolated domain, and Regime B, expansion after a section of the domain is in contact with the Plateau border (*e.g.* see Movies S1 and S2, ESI†). In Regime B, the moving front is located at the contact line between the thinner domain and thicker surrounding film. The area of isolated thinner darker isolated domains, A_d increases linearly with time. The scaling of $A_d \propto t$ has been reported and analyzed previously.[44,48] However, after the domain comes in
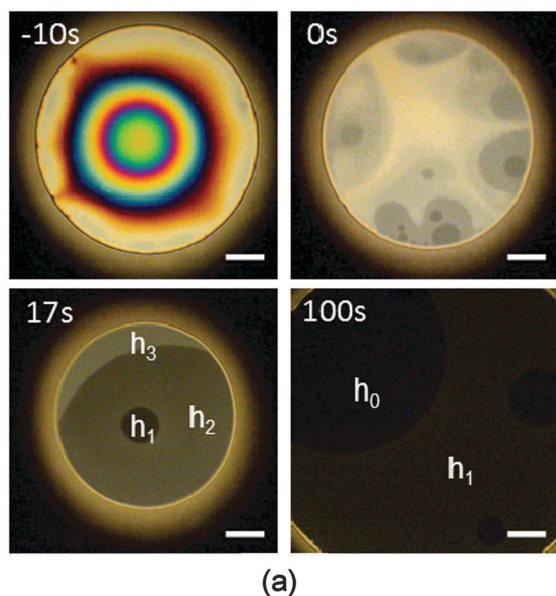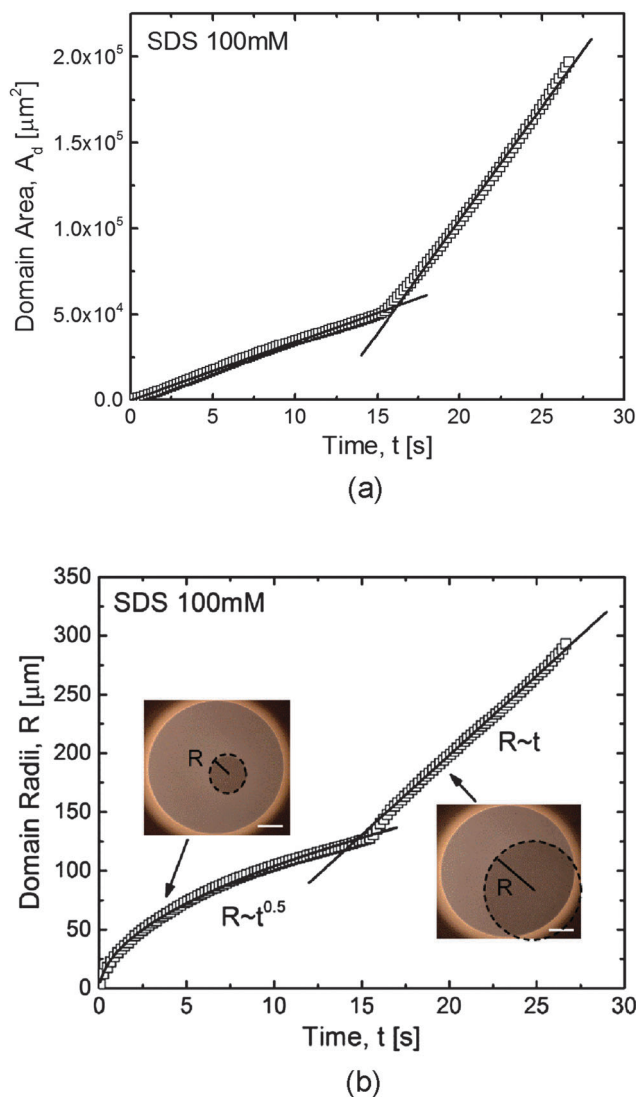
Fig. 2 Stratification (step-wise thinning) of aqueous sodium dodecyl sulfate (SDS) thin film (100 mM; c/cmc $\approx$ 12). (a) Montage of images captured using IDIOM set-up, showing the stratified thin films, and the many coexisting shades of gray represent regions of different thickness. The onset time, $t = 0$ corresponds to the instant when the last interference maxima is reached. The scale bars correspond to 100 μm (see Movie online, included as ESI†). (b) Thickness variation at the center of the film, measured by image analysis of red and green channels using IDIOM (see text for details). Thickness plateaus are labeled in correspondence with layers labeled in (a).

Fig. 3 Domain expansion dynamics in a 100 mM aqueous SDS stratifying foam film. (a) Domain area *vs.* time: The areal growth rate increases when the domain comes in contact with the surrounding Plateau border. (b) Domain radii *vs.* time: The scaling changes from $R \propto t^{0.5}$ to $R \propto t$ after the domain contacts the Plateau border. Dotted lines in the two snapshots show the domain radius R evaluated 5 s and 20 s after the domain emerged. The thickness of the expanding thin (h_1 = 26.2 nm) domain and its surrounding thicker (h_2 = 40.3 nm) film were determined using the IDIOM method. The scale bars correspond to 100 μm.

Table 1 The domain expansion dynamics is characterized by two growth rates: apparent diffusivity, D (regime A) and contact line velocity, V (regime B) respectively. The diffusivity and velocity measured are listed here for a range of concentrations for aqueous SDS solutions. In each case, the thickness of expanding domain (h_{thin}) and the thicker surrounding film (h_{thick}) is also indicated. The thickness was determined using the IDIOM method (see text for details) and the growth rates were obtained by analyzing radius *versus* time datasets

c (mM)	h_{thick} (nm)	h_{thin} (nm)	D (μm^2 s^{-1})	V (μm s^{-1})
25	41.3 ± 1.3	25.2 ± 0.4	630 ± 17	31.7 ± 3.2
32	36.5 ± 2.1	21.9 ± 1.4	710 ± 77	28.3 ± 0.9
50	32.2 ± 1.8	19.0 ± 1.4	1022 ± 72	18.8 ± 0.9
64	30.2 ± 1.6	17.7 ± 1.1	1229 ± 222	21.3 ± 2.5
	47.9 ± 2.6	30.2 ± 1.6	522 ± 22	20.3 ± 2.7
80	27.1 ± 1.9	15.3 ± 0.6	1636 ± 82	21.1 ± 3.4
	38.9 ± 3.2	27.1 ± 1.9	567 ± 133	11.6 ± 1.1
100	40.3 ± 3.6	26.2 ± 2.1	1050 ± 48	15.4 ± 2.3

expansion data in terms of the time variation of domain radius as shown in Fig. 3b. Here, a clear scaling transition from $R \propto t^{0.5}$ to $R \propto t$ is observed. The distinction between the two regimes can be now characterized and distinguished by defining two appropriate rate constants: an apparent diffusivity

$$D = \frac{dR^2}{dt} = \frac{1}{\pi}\frac{dA_d}{dt}$$ for Regime A and an apparent contact line

velocity $V = \frac{dR}{dt}$ in Regime B. These rate constants were measured for five concentrations and are summarized in the Table 1. While the apparent diffusivity measured from domain expansion in Regime A increases with concentration, the apparent velocity decreases with concentration. Practically speaking, since these two regimes show markedly different concentration dependence and time dependence, it implies that it is not easy to formulate a simple corollary on how concentration influences foam film lifetime.

3.3. Domain expansion kinetics: influence of rim instability

The radius of the expanding domain in foam films formed from a 25 mM SDS solution is tracked over time and plotted in Fig. 4. Unlike the 100 mM SDS solutions, here a transition from $R \propto t^{0.5}$ to $R \propto t$ is exhibited in the expansion kinetics of the isolated domain itself. This change in expansion kinetics occurs concomitantly with the spontaneous formation of thick white spots at the boundary between the thinner expanding domain and the surrounding film. These white spots are much thicker when compared to the surrounding film and hence appear whiter and brighter. Since their thicknesses (< 100 nm) are still much smaller than their diameters (> 10 microns), the white spots are shape-wise similar to pancakes (or lenses or discs). Consistent with the concentration dependence exhibited in other studies, stratification kinetics of the 25 mM SDS solution ($c/cmc \approx 3$) also show a larger minimum thickness with h_0 = 25.2 ± 0.4 nm and a larger step size with Δh = 16.1 ± 1.4 nm. Though the image included in Fig. 4 shows nearly uniform sized white spots arrayed all around the domain border, our extended range of experiments show that one or more white spots can appear asymmetrically about the rim (see image

contact with the Plateau border, the areal growth rate shows a marked increase (determined by the slope of curves in Fig. 3a). Though the areal growth rate changes, the linear dependence $A_d \propto t$ is preserved. Since this linear dependence of area on time has been attributed before to a diffusion-like process,[44,48] the change in slope either suggests a faster diffusion or a change in the governing dynamics. As Regime B was not characterized in the earlier experimental studies, none of the existing theoretical frameworks explicitly account for the observed change in domain expansion dynamics.

Driven to investigate why the domain expansion speeds up on contact with the Plateau border, we plotted the domain
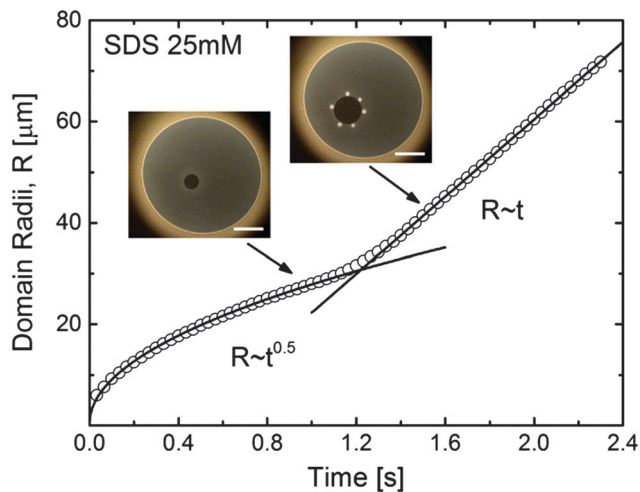
Fig. 4 Domain expansion dynamics in the 25 mM aqueous SDS solution before and after the onset of rim instability. Radius vs. time plot showing the expansion of a thinner domain (h_0 = 25.8 nm) into a surrounding thicker film (h_1 = 43.5 nm). The scaling transition took place when white spots appeared around the domain. The snapshots were taken at 1 s and 2 s after domain emerged. The scale bars correspond to 100 μm.

included in Fig. 5, for example and also see Movie S3, ESI†). In all instances, the appearance of white spots results in a change in domain expansion kinetics. Though such a transition and white spot formation are seen for 32 mM and 50 mM solutions as well, the instability leading to their formation is less likely to occur in the more concentrated SDS solutions under the conditions imposed in our experiments.

Next we analyzed the domain expansion dynamics for the cases where both white spot formation and contact with Plateau border occur successively. Two cases can be identified: Fig. 5a illustrates the case of domain expansion where rim instability leading to white spot formation occurs first, while Fig. 5b shows a case where the rim instability is initiated after contact with periphery. The similarity between the expansion dynamics observed after white spots form and after domain coalesces with Plateau border is clearly visible in Fig. 5 for both cases. The apparent velocities of domain expansion in thin films formed with 25 mM and 32 mM SDS solution are found to be very close (Table 2).

The contrast between domain expansion dynamics in the constant diffusivity regime (Regime A) and the constant velocity regime (Regime B) can be highlighted by comparing how the locus of the contact line shifts with time as shown in Fig. 6. Also shown is the change in the velocity vector. The expansion velocity varies with time for the diffusive regime (Regime A), and the magnitude of displacement is shorter in each successive (equal) time interval. In contrast, the rest of the contact line moves with a constant velocity after contact with Plateau border, and this leads to a linear growth in domain radius observed in the Regime B.

3.4. Discussion

The expansion of isolated domains in Regime A (constant diffusivity) has been observed and modeled before. Kralchevsky
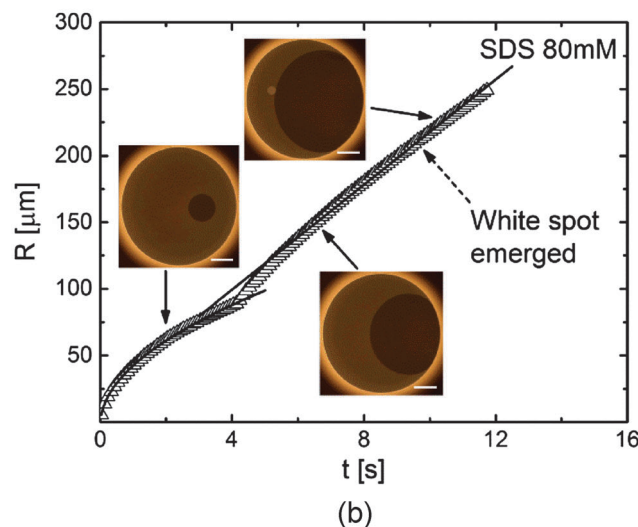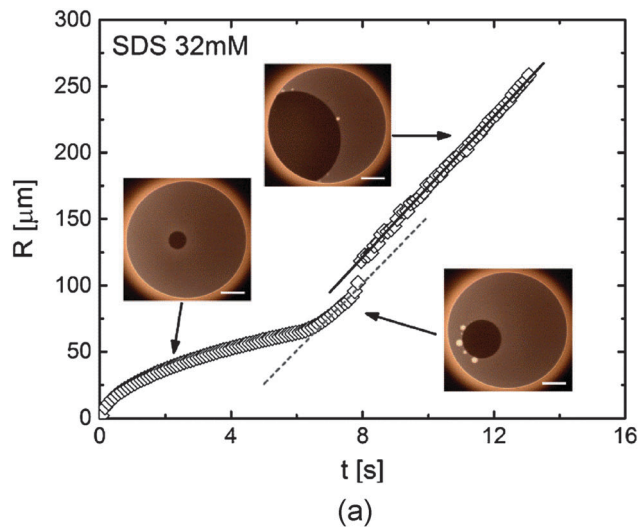

(a)

(b)

Fig. 5 Domain expansion dynamics illustrating dynamic similarity between rates after rim instability and after contacting the Plateau border. The plots show domain radii vs. time for (a) 32 mM SDS and (b) 80 mM SDS. The snapshots showing different growth scenarios were captured at 2 s, 8 s and 11 s after the domain first emerged. The scale bars bars correspond to 100 μm.

Table 2 Comparison of the contact line velocity realized after: (a) white spots appear at the domain boundary and (b) after expanding domain contacts the film periphery (Plateau border)

Concentration (mM)	h_{thick} (nm)	h_{thin} (nm)	$V_{w/spots}$ (μm s^{-1})	$V_{periphery}$ (μm s^{-1})
25	41.3 ± 1.3	25.2 ± 0.4	31.6 ± 1.2	31.7 ± 3.2
32	36.5 ± 2.1	21.9 ± 1.4	25.2 ± 3.0	28.3 ± 0.9

et al.[44] proposed a diffusive–osmotic mechanism, arguing that the chemical potential (or osmotic pressure) difference between the film and its Plateau border leads to generation of vacancies. In this model, the expansion of the thinner domains is considered akin to a phase transition, involving condensation of vacancies. Appearance of white spots, the associated change in
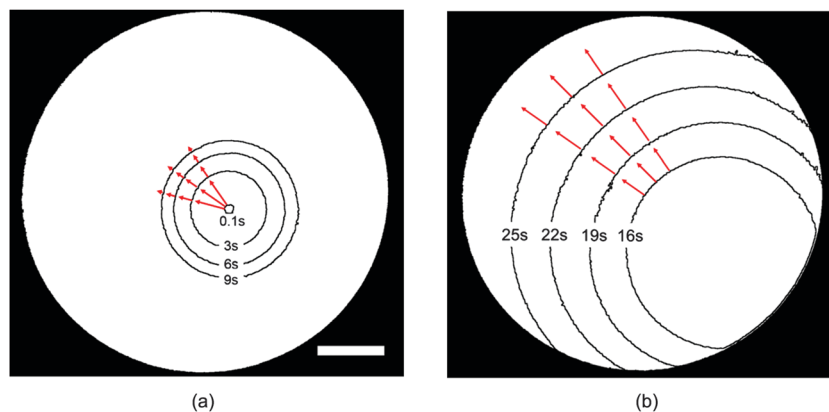
Fig. 6 The time evolution of domain boundary in the two distinct regimes. Line traces showing the position of contact line between expanding domain and thicker surroundings are obtained by image analysis. Traces with constant time interval $\Delta t = 3$ s between them are shown. Red arrows demonstrate the change in the expansion velocities at various time. (a) In Regime A, the expansion velocity decreases as the domain grows. The circles are shifted to be concentric for clarity. Here growth rate is better characterized by a constant diffusivity. (b) In Regime B, the domain boundary expands with a constant velocity. The scale bar corresponds to 100 μm.

expansion kinetics, and the constant velocity regime observed here after a domain coalesces with the Plateau border are not captured by the diffusive–osmotic mechanism. Both Bergeron and Radke,[42] and Heinig, Beltrán and Langevin[48] argue that the excess liquid from the growing thinner domain accumulates and builds a rim at the domain boundary. Heinig *et al.*[48] proposed a local diffusive model that describes how a disjoining pressure gradient across the rim drives the outwards expansion of the rim. The model arrives at a diffusive scaling for domain growth with $R \propto t^{0.5}$. Many features of their diffusive growth model are similar to the models for spreading and dewetting outlined by de Gennes, Joanny, Brochard and coworkers,[67–69] among others. However, this model is applicable only in Regime A and the dynamics observed after contact with the Plateau border as well as after formation of white spots are not captured.

Even though many studies remark that the white spots emerge due to a Rayleigh-like instability,[42,50,64,70] quantitative analysis of white spot formation and the concomitant change in domain expansion dynamics is somewhat lacking. The scaling transition $R \propto t^{0.5}$ to $R \propto t$ observed after white spot formation has been reported (we believe) only once before for polymer-free micellar dispersions. Sonin and Langevin[70] observed this change in dynamics for a dodecyltrimethylammonium bromide (DTAB) solution ($c/cmc \approx 7$). However, Beltrán and Langevin[49,50] observed similar white spot formation and change in expansion kinetics for polyelectrolyte–surfactant mixtures. By drawing analogy with spreading kinetics, Beltrán and Langevin[50] posited that the constant velocity near the contact line could be a result of a balance between viscous dissipation and the uncompensated Young force. However, the estimated values for velocity are nearly three orders of magnitude smaller than the values obtained from experiments.

Recognizing the discrepancy, Beltrán and Langevin[50] argued that a better estimate of the contact line velocity is obtained if the gain in surface energy associated with white spot formation due to Rayleigh instability is considered as the driving force.

Furthermore, it was argued that the effective viscosity of polyelectrolyte solution is two orders of magnitude smaller than the bulk viscosity. In contrast, the model for diffusive regime proposed by Heinig, Beltrán and Langevin[48] captures the experimentally observed dynamics only if a viscosity enhancement (again by two orders) is assumed. Since these two studies from the Langevin group[48,50] were carried out for polyelectrolyte–surfactant mixtures, it is possible that polymer viscoelasticity and shear-rate dependent viscosity play a role. Nonetheless, a self-consistent explanation of the contrasting dynamics observed in two regimes remains a challenge even for the polymer-free micellar fluids. The complexity arises because both thermodynamic and hydrodynamic effects are involved and must be carefully considered for the case of confined fluids.

In contrast to the previous studies,[10,36,39–44,48–50,53–55] our experiments on domain expansion dynamics lead to three distinct observations that need to described by a theoretical framework self-consistently: (i) The dynamics change from constant diffusivity (Regime A) to constant contact line velocity (Regime B) mode after an isolated domain comes in contact with the Plateau border (see Fig. 3, 5 and 6); (ii) Though the apparent diffusivity increases with surfactant concentration in Regime A, the contact line velocity shows a decrease over the same concentration range (see Table 1); (iii) Even though the change in dynamics from constant diffusivity to constant velocity that is observed after the onset of topological instability has been reported a countable few times before,[49,50,70] there is no indication that such a transition could occur after the domain contacts Plateau border. Even so, it remains to be explained why a similar contact line velocity is realized in both cases (see Fig. 5 and 6; Table 2). We have developed a theoretical framework, which captures the scaling behavior displayed in both regimes, as well as the concentration dependence of growth rates (diffusivity and velocity respectively). The theory will be presented with necessary details in the next paper, but the key ideas are summarized next.

The thin film hydrodynamics in both regimes can be described using the following thickness evolution equation:[71–73]

$$\frac{\partial h}{\partial t} = \frac{1}{12\eta r}\frac{\partial}{\partial r}\left(rh^3\frac{\partial P}{\partial r}\right) \qquad (3)$$

This evolution equation for foam film thickness $h(r,t)$ is derived from the Navier–Stokes equation using a lubrication flow assumption (valid for $h \ll R$). The relevant pressure for thin films is obtained from the Derjaguin equation:[73] $P = \gamma C + \Pi$ that includes contributions from the capillary pressure (depends on surface tension and local curvature, C) and the disjoining pressure, $\Pi(h)$. In the case of the stratifying foam films, the thickness-dependent interaction potential $f(h)$ (and disjoining pressure $\Pi = -\partial_h f(h)$) display a highly non-monotonic behavior. The nucleation and growth of successively thinner domains and the stepwise thinning can be understood as being driven by a progressive transition from one metastable state to the next made possible by the oscillatory nature of a thickness-dependent free energy isotherm.[18,44–47] Domains of different thicknesses can coexist within the same foam film as the thickness-dependent osmotic pressure generated by the surface forces (or disjoining pressure) can equilibrate with the global Laplace pressure (given by eqn (1), and set by the film size).

Initial growth of domains involves a rapid outflow, leading to an accumulation of fluid near the domain boundary, which creates an asymmetric, nearly flat rim. In this case, the gradient in disjoining pressure makes the primary contribution to the driving force for the outflow and the dissipation within the rim controls the expansion dynamics (in analogy with spreading and dewetting literature[67–69]). The height evolution equation resembles a diffusion equation $\partial_t h = D_{\text{eff}}\nabla^2 h$ with $D_{\text{eff}} = -\frac{h_\infty^3}{12\eta}\frac{\partial\Pi}{\partial h}$ where η is the viscosity and h_∞ is the thickness of the surrounding film. The diffusive transport of fluid through the rim results in an increase in both rim height and rim width. We experimentally observe that beyond a critical height, the rim is unstable, and breaks-up into white spots (see Movie S3, ESI†). Due to the non-monotonic nature of the disjoining pressure curve and the Laplace pressure associated with non-flat surfaces, the rim evolves towards this critical height, and the dynamics get progressively slower as the critical height is approached. We find that the apparent velocity of the contact line in regime A decreases with time as $V_A \propto t^{-0.5}$ and is slowest before the onset of instability. Alternatively, the growing domain impinges on the Plateau border before the onset of rim instability. For both these scenarios, the transition is accompanied by a noticeable jump in the contact line velocity, and the constant diffusivity regime is followed by a constant velocity regime.

In the mechanism proposed by Beltrán and Langevin,[50] the growth of white spots by Rayleigh instability and surface energy as driving force are said to drive the constant velocity expansion. After a careful analysis of innumerable movies (see ESI,† Movie S2), we find that the rim break-up is often not symmetric and the white spots (nearly flat, similar to pancakes rather than drops) do not display periodicity or growth rates associated with the Rayleigh instability. The emergence and growth of white spots show instability evolution and morphologies that are strikingly different from the Rayleigh break-up of toroidal rings into droplets.[74,75] Arguably the differences arise as the formation of white spots occurs near an expanding contact line, and unlike toroidal rings, the rims formed in foam films do not have a circular cross-section and are always connected to a thinner and a thicker film. The growing white spots can move along the expanding domain boundary, coalesce with each other, and their complex dynamics (see Movie S3, ESI† for example) have not been described before. We infer that the forces and fluxes responsible for rim evolution and growth, as well as topological instability, require more scrutiny.

We have pointed out in the earlier sections that after a domain contacts the Plateau border, both the scaling law exponent and the contact line velocity are quite similar to the values obtained after the onset of topological instability that leads to the formation of white spots (see Table 2). In both instances, the thinner domain grows at the expense of the thicker domain, without any apparent outward flow from the thin domain. The rim instability and contact with the Plateau border both trigger a change in dynamics such that diffusive term based on disjoining pressure plays a secondary role in regime B. Here the dissipation occurs within the transition region that connects the growing thinner domain to thicker, less metastable surrounding film. Though some similarity exists with dewetting dynamics and phase separation kinetics in thin films,[67–69,71–73] a detailed framework is needed that accounts for the rim shape and evolution in free-standing films with careful consideration of free energy and disjoining pressure that display a highly non-monotonic, thickness dependence. We will present the detailed model in a later publication, and articulate how the choice of surfactant, micelle concentration and overall coupling of hydrodynamics and thermodynamics influences the domain growth dynamics.

4. Conclusions

We examined stratification in thin foam films containing sodium dodecyl sulfate (SDS) micelles using a novel technique, Interferometry Digital Imaging Optical Microscopy (IDIOM), which was developed as a part of this study. We successfully measured the thickness of the thin films down to ~ 10 nm with high accuracy from intensity mapping and interferometry analysis of images recorded by a digital camera. The technique IDIOM allows for a simultaneous measurement of drainage kinetics and domain expansion dynamics, providing a powerful tool for studying instabilities and dynamic processes that accompany stratification.

Stratification or stepwise thinning in micellar fluids occurs through spontaneous formation and growth of thinner, hence visibly darker, circular domains. The domain expansion dynamics were analyzed by tracking the location of the contact line between a thinner domain and its surrounding thicker film.

In agreement with published studies, the radius of an isolated domain grows as $R \propto t^{0.5}$, displaying a constant apparent diffusivity. After a section of the growing domain impinges on the Plateau border, the contact line between the thin domain and its thicker surroundings moves with a constant velocity. In contrast with the $R \propto t^{0.5}$ behavior (Regime A) that has been observed and modeled before, this constant velocity regime with contact line displaying $R \propto t$ (Regime B) is identified and characterized for the first time. The transition from a constant diffusivity to a constant velocity regime can also be observed in the expansion kinetics of an isolated domain whenever a topological instability occurs that leads to the formation of thicker white spots near the contact line between expanding domain and thicker surroundings.

Several observations included in this study require a thorough investigation of hydrodynamic and thermodynamic effects that contribute to domain formation and expansion in micellar films. In particular, a self-consistent theoretical framework is needed to capture the change from a constant diffusivity to a constant velocity regime and for *a priori* estimation of these growth rates in the two regimes for different surfactants. On varying the concentration of SDS micelles, we observed that apparent diffusivity increases with concentration, while the apparent velocity decreases with concentration. A theoretical model that describes the mechanistic basis of the two regimes, as well as the concentration dependence of growth rates displayed in each case, will be the focus of the second paper in this series.

Acknowledgements

References

1 S. Perkowitz, *Universal Foam: from Cappuccino to the Cosmos*, Walker & Company, 2000.
2 R. Backov, *Soft Matter*, 2006, **2**, 452–464.
3 R. Mezzenga, P. Schurtenberger, A. Burbidge and M. Michel, *Nat. Mater.*, 2005, **4**, 729–740.
4 *Foams: Theory, Measurements, and Applications*, ed. R. K. Prud'homme and S. A. Khan, CRC Press, 1995.
5 D. L. Weaire and S. Hutzler, *The Physics of Foams*, Oxford University Press, 1999.
6 A. Saint-Jalmes, *Soft Matter*, 2006, **2**, 836–849.
7 I. B. Ivanov, *Thin Liquid Films: Fundamentals and Applications*, CRC Press, 1988.
8 D. Langevin, *ChemPhysChem*, 2008, **9**, 510–522.
9 A. Sheludko, *Adv. Colloid Interface Sci.*, 1967, **1**, 391–464.
10 I. Cantat, S. Cohen-Addad, F. Elias, F. Graner, R. Höhler and O. Pitois, *Foams: Structure and Dynamics*, Oxford University Press, 2013.

11 D. Fennell Evans and H. Wennerström, *The Colloidal Domain: Where Physics, Chemistry, Biology, and Technology Meet*, Wiley-VCH, New York, 2nd edn, 1999.
12 S. A. Magrabi, B. Z. Dlugogorski and G. J. Jameson, *Fire Saf. J.*, 2002, **37**, 21–52.
13 T. J. Martin, *Foam Engineering: Fundamentals and Applications*, 2011, pp. 411–457.
14 S. Farrokhpay, *Adv. Colloid Interface Sci.*, 2011, **166**, 1–7.
15 R. J. Pugh, *Adv. Colloid Interface Sci.*, 1996, **64**, 67–142.
16 A. Bureiko, A. Trybala, N. Kovalchuk and V. Starov, *Adv. Colloid Interface Sci.*, 2014, DOI: 10.1016/j.cis.2014.10.001.
17 *Rheological Properties of Cosmetics and Toiletries*, ed. D. Laba, Marcel Dekker, Inc, New York, 1993.
18 V. Bergeron, *J. Phys.: Condens. Matter*, 1999, **11**, R215.
19 G. Liger-Belair, G. Polidori and P. Jeandet, *Chem. Soc. Rev.*, 2008, **37**, 2490–2511.
20 K. Schilling and M. Zessner, *Water Res.*, 2011, **45**, 4355–4366.
21 A. Bridie, T. H. Wanders, W. Zegveld and H. B. Van der Heijde, *Mar. Pollut. Bull.*, 1980, **11**, 343–348.
22 K. J. Mysels, S. Frankel and K. Shinoda, *Soap films: Studies of their Thinning and a Bibliography*, Pergamon Press, 1959.
23 H. A. Stone, S. A. Koehler, S. Hilgenfeldt and M. Durand, *J. Phys. Condens. Matter*, 2003, **15**, S283–S290.
24 M. Safouane, A. Saint-Jalmes, V. Bergeron and D. Langevin, *Eur. Phys. J. E: Soft Matter Biol. Phys.*, 2006, **19**, 195–202.
25 J. F. Sadoc and N. Rivier, *Foams and Emulsions*, Springer, 1999.
26 D. Georgieva, A. Cagna and D. Langevin, *Soft Matter*, 2009, **5**, 2063–2071.
27 S. Costa, R. Höhler and S. Cohen-Addad, *Soft Matter*, 2013, **9**, 1100–1112.
28 V. Bergeron and C. J. Radke, *Langmuir*, 1992, **8**, 3020–3026.
29 B. V. Derjaguin, N. V. Churaev and V. M. Muller, *Surface Forces*, Springer, New York, 1987.
30 C. Stubenrauch and R. von Klitzing, *J. Phys.: Condens. Matter*, 2003, **15**, R1197.
31 A. D. Nikolov and D. T. Wasan, *Adv. Colloid Interface Sci.*, 2014, **206**, 207–221.
32 N. D. Denkov, S. Tcholakova, K. Golemanov, K. Ananthpadmanabhan and A. Lips, *Soft Matter*, 2009, **5**, 3389–3408.
33 S. Cohen-Addad, R. Hohler and O. Pitois, *Annu. Rev. Fluid Mech.*, 2013, **45**, 241–267.
34 A. Salonen, W. Drenckhan and E. Rio, *Soft Matter*, 2014, **10**, 6870–6872.
35 L. Saulnier, J. Boos, C. Stubenrauch and E. Rio, *Soft Matter*, 2014, **10**, 7117–7125.
36 H. Fauser and R. von Klitzing, *Soft Matter*, 2014, **10**, 6903–6916.
37 A. Maestro, E. Rio, W. Drenckhan, D. Langevin and A. Salonen, *Soft Matter*, 2014, **10**, 6975–6983.
38 J. Israelachvili, *Intermolecular and Surface Forces*, Academic Press, San Diego, 2nd edn, 1992.
39 A. D. Nikolov and D. T. Wasan, *J. Colloid Interface Sci.*, 1989, **133**, 1–12.

40 A. D. Nikolov, P. A. Kralchevsky, I. B. Ivanov and D. T. Wasan, *J. Colloid Interface Sci.*, 1989, **133**, 13–22.

41 A. D. Nikolov, D. T. Wasan, P. A. Kralchevsky and I. B. Ivanov, in *Ordering and Organization in Ionic Solutions*, ed. N. Ise and I. Sogami, World Scientific, Singapore, 1988.

42 V. Bergeron, A. I. Jimenez-Laguna and C. J. Radke, *Langmuir*, 1992, **8**, 3027–3032.

43 D. T. Wasan and A. D. Nikolov, *Curr. Opin. Colloid Interface Sci.*, 2008, **13**, 128–133.

44 P. A. Kralchevsky, A. D. Nikolov, D. T. Wasan and I. B. Ivanov, *Langmuir*, 1990, **6**, 1180–1189.

45 D. Langevin, C. M. Beltran and J. Delacotte, *Adv. Colloid Interface Sci.*, 2011, **168**, 124–134.

46 K. D. Danov, E. S. Basheva, P. A. Kralchevsky, K. P. Ananthapadmanabhan and A. Lips, *Adv. Colloid Interface Sci.*, 2011, **168**, 50–70.

47 S. E. Anachkov, K. D. Danov, E. S. Basheva, P. A. Kralchevsky and K. P. Ananthapadmanabhan, *Adv. Colloid Interface Sci.*, 2012, **183–184**, 55–67.

48 P. Heinig, C. M. Beltrán and D. Langevin, *Phys. Rev. E: Stat., Nonlinear, Soft Matter Phys.*, 2006, **73**, 051607.

49 C. M. Beltrán, S. Guillot and D. Langevin, *Macromolecules*, 2003, **36**, 8506–8512.

50 C. M. Beltrán and D. Langevin, *Phys. Rev. Lett.*, 2005, **94**, 217803.

51 E. S. Johonnott, *Philosophical Magazine Series 6*, 1906, vol. 11, pp. 746–753.

52 J. Perrin, *Ann. Phys. (Paris, Fr.)*, 1918, **10**, 160–184.

53 A. D. Nikolov and D. T. Wasan, *Colloids Surf., A*, 1997, **128**, 243–253.

54 G. N. Sethumadhavan, A. D. Nikolov and D. T. Wasan, *Langmuir*, 2001, **17**, 2059–2062.

55 A. D. Nikolov, D. T. Wasan and S. E. Friberg, *Colloids Surf., A*, 1996, **118**, 221–243.

56 M. J. Rosen and J. T. Kunjappu, *Surfactants and Interfacial Phenomena*, John Wiley & Sons, 2012.

57 A. M. Poskanzer and F. C. Goodrich, *J. Phys. Chem.*, 1975, **79**, 2122–2126.

58 K. J. Mysels, *Langmuir*, 1986, **2**, 423–428.

59 E. A. Adelizzi and S. M. Troian, *Langmuir*, 2004, **20**, 7482–7492.

60 S. Berg, E. A. Adelizzi and S. M. Troian, *Langmuir*, 2005, **21**, 3867–3876.

61 S. I. Karakashev, A. V. Nguyen and E. D. Manev, *J. Colloid Interface Sci.*, 2007, **306**, 449–453.

62 S. Sett, S. Sinha-Ray and A. L. Yarin, *Langmuir*, 2013, **29**, 4934–4947.

63 D. Exerowa, T. Kolarov and K. Khristov, *Colloids Surf.*, 1987, **22**, 161–169.

64 V. Bergeron and C. J. Radke, *Colloid Polym. Sci.*, 1995, **273**, 165–174.

65 L. G. Cascão Pereira, C. Johansson, H. W. Blanch and C. J. Radke, *Colloids Surf., A*, 2001, **186**, 103–111.

66 S. E. Anachkov, K. D. Danov, E. S. Basheva, P. A. Kralchevsky and K. P. Ananthapadmanabhan, *Adv. Colloid Interface Sci.*, 2012, **183–184**, 55–67.

67 F. Brochard-Wyart and J. Daillant, *Can. J. Phys.*, 1990, **68**, 1084–1088.

68 J. F. Joanny and P. G. de Gennes, *J. Phys.*, 1986, **47**, 121–127.

69 L. Leger and J. F. Joanny, *Rep. Prog. Phys.*, 1992, **55**, 431.

70 A. A. Sonin and D. Langevin, *Europhys. Lett.*, 1993, **22**, 271.

71 L. G. Leal, *Advanced Transport Phenomena: Fluid Mechanics and Convective Transport Processes*, Cambridge University Press, 2007.

72 U. Thiele, *Thin Films of Soft Matter*, SpringerWien, New York, 2007.

73 V. M. Starov, M. G. Velarde and C. J. Radke, *Wetting and Spreading Dynamics*, CRC Press, New York, 2007.

74 E. Pairam and A. Fernández-Nieves, *Phys. Rev. Lett.*, 2009, **102**, 234501.

75 Z. Zhang, G. C. Hilton, R. Yang and Y. Ding, arXiv preprint arXiv:1502.03207, 2015.